OPEN ACCESS
Fluctuation and Noise Letters
(2026) 2540027 (12 pages)

DOI: 10.1142/S0219477525400279

Toward Sensing Protein Interactions and Dynamics via $1/f$ Noise in Graphene Field-Effect Transistors

M. Fomin*, F. Steinbach*,§, D. Pustovyi†, N. Füllbrunn‡, K. Tanzusch‡, C. You‡, C. Ungermann‡, S. Vitusevich†, M. Petrychuk† and C. Meyer*,¶

*Department of Mathematics/Computer Science/Physics, Institute of Physics
University of Osnabrück, D-49069 Osnabrück, Germany

†Institute of Biological Information Processing (IBI-3), Forschungszentrum Jülich
D-52428 Jülich, Germany

‡Department of Biology/Chemistry and Center for Cellular Nanoanalytics
University of Osnabrück
Osnabrück D-49069, Germany

§fsteinbach@uni-osnabrueck.de

¶carola.meyer@uni-osnabrueck.de

Received 2 May 2025
Revised 13 November 2025
Accepted 23 November 2025
Published 28 February 2026

Communicated by Aneta Stefanovska

Graphene field-effect transistors (GFETs) functionalized with lipid monolayers provide a sensitive platform for probing membrane protein dynamics. Here, we analyze the effect of peripheral membrane proteins on this assay. We focused on the prenylated Rab7 GTPase Ypt7 and its interacting HOPS tethering complex using liquid-gated GFETs combined with low-frequency noise spectroscopy. Current–voltage (I–V) transfer measurements reveal no or only very small changes upon binding of Ypt7 and after addition of HOPS. In contrast, noise analysis reveals pronounced flicker ($1/f$) noise level growth after Ypt7 binding, most likely due to conformational dynamics of Ypt7. Recruitment of the HOPS complex by Ypt7 to membranes inhibits these fluctuations, suggesting structural stabilization of Ypt7 via HOPS binding. Our findings demonstrate that noise spectroscopy allows for enhancing the sensitivity of GFET-based biosensing, offering insights into protein–membrane and protein–protein interactions beyond traditional electronic readouts.

Keywords: $1/f$ noise; Graphene field-effect transistor; HOPS complex; membrane proteins; Rab GTPases.

¶Corresponding author.

1. Introduction

Graphene-based field-effect transistors (GFETs) have emerged as a powerful platform for biosensing due to their exceptional electronic properties, including high carrier mobility, chemical stability, and two-dimensional nature, which together enable extreme sensitivity to interfacial perturbations [1, 2]. When operated in a liquid-gated configuration, GFETs can transduce biochemical interactions occurring at the surface into measurable electrical signals, offering a label-free, real-time readout [3–5].

More than one-third of the proteome in animal cells localizes to cellular membranes. Notably, most therapeutic drugs target these membrane proteins [6]. Exploring functions and interactions of membrane proteins requires a native membrane environment as well as high spatiotemporal resolution. Compared to traditional biological methods, fluorescence spectroscopy and microscopy methods provide high sensitivity down to single molecule level. However, these approaches need dedicated quality control on fluorescent labeling of the target proteins [7]. Electrical biosensing is an emerging, powerful tool for the investigation of membrane-associated biological processes [8, 9]. Recent advances highlight the integration of supported lipid bilayers and monolayers with carbon-based materials, offering a promising strategy to mimic native membrane environments for sensitive, label-free detection while maintaining protein functionality [3, 10–12].

We focus on understanding the dynamic behavior of Rab GTPases and their effector proteins, such as the yeast Rab7-like Ypt7 and the homotypic fusion and vacuole protein sorting (HOPS) tethering complex, in the context of lipid-functionalized GFETs. Rab proteins, including Ypt7, are essential regulators of membrane trafficking processes [13–15]. Immobilizing Ypt7 on supported lipid monolayers allows us now to probe not only its electrostatic signature but also its conformational dynamics through noise spectroscopy, a technique sensitive to molecular fluctuations at bioelectronic interfaces [16, 17].

Moreover, the binding of multi-protein assemblies such as the HOPS tethering complex to membrane-bound Ypt7 provides a unique opportunity to monitor protein–protein interactions (PPI) in a near-native state. Previous studies have resolved the architecture and functional dynamics of HOPS using optical and biochemical methods [12, 18], but integration of electronic readout schemes like GFETs introduces a new level of temporal resolution and label-free detection capability.

In this work, we present a detailed fabrication and functionalization protocol for GFETs decorated with a lipid monolayer, followed by subsequent immobilization of Ypt7 and the HOPS complex. We employ I–V transfer characteristics and low-frequency noise analysis to distinguish each functionalization step and extract insights into molecular interactions occurring at the graphene–lipid–protein interface. Our approach builds on liquid-gated graphene transistors to probe biomolecular dynamics [19], providing a powerful tool to understand the vesicle tethering and fusion machinery dynamics in the context of biological membranes.

2. Materials and Methods

2.1. *Liquid-gated graphene field-effect transistors*

The fabrication process of graphene-based field-effect transistors (GFETs) followed a well-established procedure described in detail in our previous work [3].

The schematic structure of the device is shown in Fig. 1(a), illustrating the graphene channel on a SiO2/p–Si substrate with Ti/Au contacts passivated to form a gate window for liquid measurements. Transistors were fabricated on p-doped silicon wafers with a 200 nm silicon dioxide layer. Graphene (Easy Transfer, G/P-25–25, Graphenea, Spain) was transferred to the substrates using a wet transfer technique. After removing a sacrificial layer, the graphene was patterned using oxygen plasma reactive ion etching (100 W, 3 min). Metal feedlines and contacts were passivated in a subsequent step, while openings for liquid gating over the graphene channels were created. Figure 1(b) shows the fabricated devices in an image taken with an optical microscope. The distance between the contacts was designed to be $d = 20\,\mu$m, with channel widths ranging from 10 to 1 μm. The device used in this study had a channel width of 2 μm. After fabrication, the chips were wire-bonded onto leadless chip carriers and encapsulated with PDMS to form a reservoir for long-term measurements.

2.2. *Functionalization of GFETs and immobilization of proteins*

2.2.1. *Formation of lipid monolayer on GFETs*

To functionalize the graphene field-effect transistor (GFET) channel, we employed the established protocols to form a supported lipid monolayer [10]. Small unilamellar vesicles (SUVs) were prepared from 1,2-dioleoyl-sn-glycero-3-phosphocholine (DOPC) (Avanti Polar Lipids, USA) using probe sonication in a buffer solution (50 mM HEPES, pH 7.5, 150 mM NaCl), as previously described [12]. The obtained SUV solution with a DOPC lipid concentration of 250 μM was added to the GFET channel and incubated for 30 min, followed by extensive buffer washes to remove unbound vesicles. During this process, the strong hydrophobicity of graphene

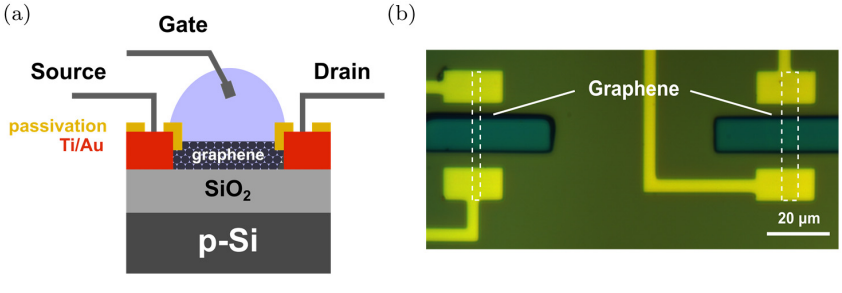

Fig. 1. (a) Schematic illustration of the fabricated GFETs structure. (b) Optical images of fabricated devices showing the tentative locations of graphene channels (indicated by white dashed boxes) with designed widths of 4 and 8 μm, from left to right, respectively.

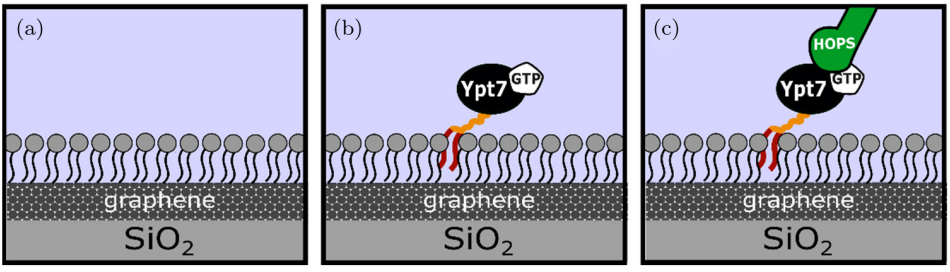

Fig. 2. Schematic illustration of the graphene channel surface at each step: (a) formation of a DOPC lipid monolayer, (b) activation and immobilization of Ypt7 and (c) binding of the HOPS complex (here: schematic representation of the Ypt7-binding subunit Vps39 of the complex). The hypervariable domain of Ypt7 shown in orange follows the prenyl anchor in red. GTP is located at the nucleotide-binding pocket.

induced liposome disruption and self-assembly of a lipid monolayer with a thickness of ∼2.5 nm on the graphene surface [10], as sketched in Fig. 2(a).

2.2.2. *Immobilization of Ypt7 and the HOPS complex*

Following lipid monolayer formation, we immobilized the Rab GTPase Ypt7 on the GFET surface. The Ypt7-GDI complex was prepared according to Füllbrunn *et al.* [12] and chemically activated via EDTA/GTP treatment in the presence of the lipid monolayer. Last, the anchoring to the lipid monolayer was stabilized by the addition of $MgCl_2$ (Fig. 2(b)). In detail, 150 nM Ypt7-GDI complex (24.2 μL) was mixed with 1 mM GTP (5 μL) and 20 mM EDTA (20 μL) and filled up with HEPES buffer (HBS) to a total volume of 500 μL. This mixture was applied to the GFET surface, followed by incubation for 30 min. Afterwards, 25 mM MgCl2 (12.5 μL) was added, followed by an additional 10 min incubation and extensive buffer washing (15 times) to dilute the remaining soluble components (to ∼0.003%).

Upon immobilization of Ypt7, 50 nM HOPS tethering complex (27.8 μL filled up with HBS to 500 μL) purified according to Shvarev *et al.* [18] was added to the functionalized surface for 10 min, followed by a five-fold buffer wash to remove unbound proteins (Fig. 2(c)).

2.2.3. *Noise measurements*

The noise spectroscopy setup used for the study is built around the Agilent U2542A data acquisition unit and designed for high-precision voltage noise measurements in nanostructures.

During measurement, signals from the device under experiment are amplified using a custom ultra-low-noise amplifier, followed by a cascade of commercial amplifiers (e.g., ITHACO 1201 and PGA-103) with programmable gain up to × 100,000. The amplified signal is filtered with a digitally controlled anti-aliasing filter (LTC1564) with a selectable cutoff frequency from 10 to 150 kHz. Noise was recorded in AC mode, digitized with a 500 kHz sampling rate in the frequency range from 10 to 100 kHz.

The acquisition time for the noise measurements was set to 300 s, exceeding the 100 s threshold below which the influence on the characteristics of $1/f$ noise is considered negligible.

The measurement error can be determined as

$$\varepsilon = 100\% \frac{\Delta t}{T} \tag{1}$$

where T is the acquisition time and $\Delta t = 1\,\text{s}$ represents the sampling interval.

This gives us a measurement error of 6%, which remains well below the commonly accepted limit of 10% for experimentally obtained results.

Noise spectroscopy revealed slight leakage noise, especially at frequencies over 10 kHz. To account for this, leakage noise spectra were measured separately for each step ($V_{\text{DS}} = 0\,\text{V}$) and subtracted from the useful signal before data analysis.

After leakage noise subtraction, the measured voltage was converted to current noise spectral density utilizing the following equation:

$$S_I(f) = \frac{S_V(f)}{R_{\text{eq}}^2}. \tag{2}$$

Here, R_{eq} is an equivalent resistance comprised of the parallel connection of channel resistance R_{ch} and load resistance R_{Load} (500 Ω).

All measurements were carried out at room temperature.

3. Results

The functionalization process was monitored using *I–V* transfer measurements and noise spectroscopy. To ensure accurate results, each measurement was conducted after a buffer wash at every step, removing excess molecules.

3.1. *I–V transfer measurements*

The *I–V* transfer curves are shown in Fig. 3. They are normalized with respect to the current level of the charge neutrality point (CNP) of the pristine device to focus on the shift of the CNP as well as changes in the transconductance (Fig. 3(b)). We observed a decrease in the current level at the CNP of 60 μA after lipid layer formation, as well as after Ypt7 activation. The current level remained constant during the subsequent functionalization steps. We attribute this small increase in resistance to the introduction of scattering centers originating from the attachment of molecules directly or close to the graphene channel (Figs. 2(a) and 2(b)).

On the other hand, the HOPS complex does not get in direct contact with the graphene channel but is bound to the membrane-anchored Ypt7 (Fig. 2(c)). Therefore, as observed but not shown, no change in resistance is expected.

The transconductance was extracted as the first-order derivative of the normalized *I–V* transfer curves, following the relation $g_m = dI/dV$.

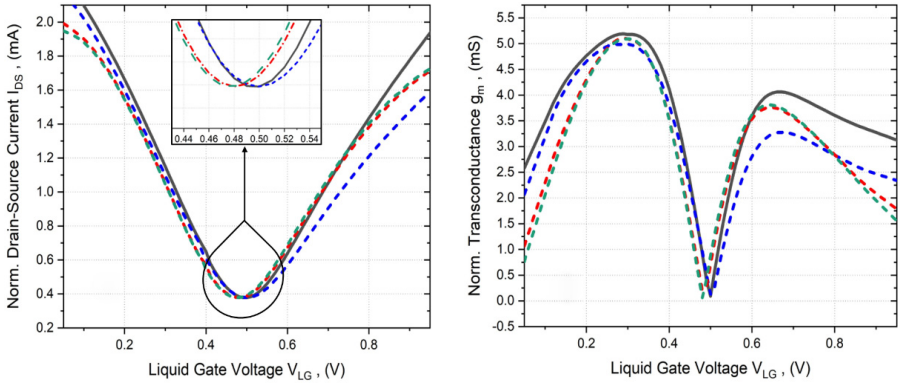

(a) (b)

Fig. 3. (a) Current–voltage (I–V) transfer characteristics with the inset showing a zoomed-in view around the charge neutrality point and (b) transconductance characteristics measured after HBS buffer wash at each functionalization step, with bias voltage $V_{SD} = 100\,\text{mV}$. Key: black solid — pristine device, blue short dash — after lipid monolayer formation, red dash-dot — after Ypt7 activation and attachment, green long dash — after HOPS complex immobilization.

The CNP voltage (V_{CNP}) remains unchanged after formation of the DOPC lipid monolayer. This stability is attributed to the zwitterionic nature of the DOPC lipids. However, a decrease in the maximum of the transconductance is observed, suggesting that the lipid monolayer may induce a non-uniform carrier transport effect across the graphene surface, leading to a slight transconductance reduction [20].

Ypt7 activation led to a $-20\,\text{mV}$ shift in the CNP, consistent with an electrostatic effect associated with positive charge originating from the protein or its positively charged regions near the channel.

In contrast, immobilization of the HOPS complex had negligible effects on the CNP position and on the transconductance. This limited electrostatic impact may be due to the large size and the distant positioning of the HOPS complex from the graphene channel. The electrostatic sensitivity of the device is constrained by the ionic concentration of the buffer [21]. Given that $1 \times$ HBS buffer was used, the highest electrostatic sensitivity is achievable within 0.75 nm of the channel according to the Debye length, beyond which sensitivity declines exponentially. Changes of the capacitance can be observed beyond the Debye length if a Donnan potential is formed [22]. However, the absence of changes in source-drain current (not shown) and in the transconductance, as shown in Fig. 3(b) suggest that the capacitance remains mainly unaffected by protein attachment. At the same time, noise spectroscopy allows us to obtain more detailed information, as will be shown below.

3.2. *Noise measurements*

In addition to I–V transfer characterization, noise measurements were conducted to investigate the effects of each functionalization step.

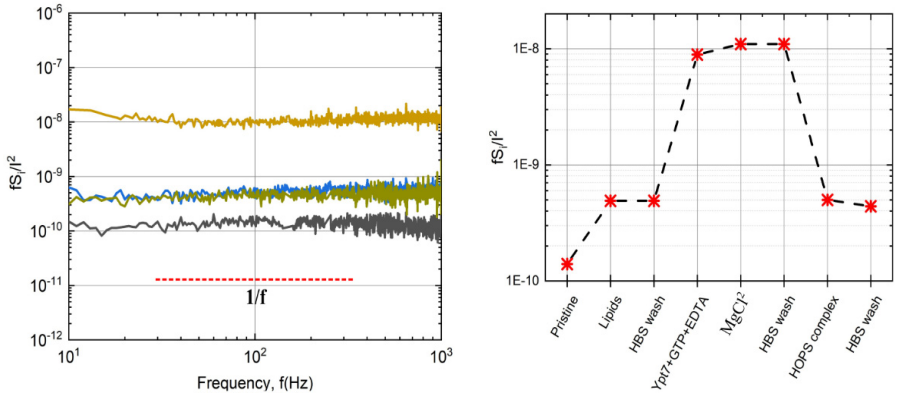

Fig. 4. (a) Normalized noise spectral densities for each functionalization/immobilization step after buffer wash, with bias voltage $V_{DS} = 0.1\,V$, and with gate voltage $V_{LG} = 0.1\,V$. Key: Black — pristine device, blue — after lipid monolayer formation, yellow — after Ypt7 activation and attachment, green — after HOPS complex immobilization. Note that noise spectra are normalized to frequency, the red dashed line indicating $1/f$ noise. (b) Corresponding noise level changes for each functionalization step.

Following the formation of the lipid monolayer, a significant increase in the normalized noise spectral density fS_i/I^2 was observed, rising from 1.4×10^{-10} to 4.9×10^{-10} (Fig. 4). After activation of Ypt7, the overall noise level exhibited a significant rise from 4.9×10^{-10} to 8.9×10^{-9} fS_i/I^2. This level remains almost constant during the stabilization of the anchoring in the lipid monolayer as well as after removing the excess molecules (Fig. 4(b)). Ypt7 activation and recruitment onto the lipid monolayer requires an incubation for 30 min. During this activation process, Ypt7 first undergoes a nucleotide binding pocket remodeling, which involves structural changes in the nucleotide binding pocket. The removal of Mg^{2+} by EDTA destabilizes in particular the important Switch I and Switch II regions in Ypt7, which are located next to the nucleotide binding pocket, thereby enabling the exchange of GDP for GTP [13]. This transition allows Ypt7 to adopt its active state and anchor to the lipid monolayer. Subsequently, the addition of MgCl2 as a source of Mg^{2+} ions stabilizes the nucleotide binding to Ypt7 and allows for HOPS binding.

To study the origin of the fluctuations causing the noise, the gate dependence of the noise spectral density levels was measured. The results are presented in Fig. 5. They reveal that changes in the overall noise level for different functionalization steps remain consistent across different gate voltages, demonstrating the stability of the biosensor response. The noise reaches its maximum at the CNP, indicating a stronger contribution from carrier capture–emission events in regions of lower carrier density. The linear decrease of the noise level to both sides of the CNP is consistent with the linear increase of the charge carrier density in graphene. This behavior supports the hypothesis that functionalization-induced charge fluctuations play a critical role in the observed noise characteristics of the system. Recent studies using

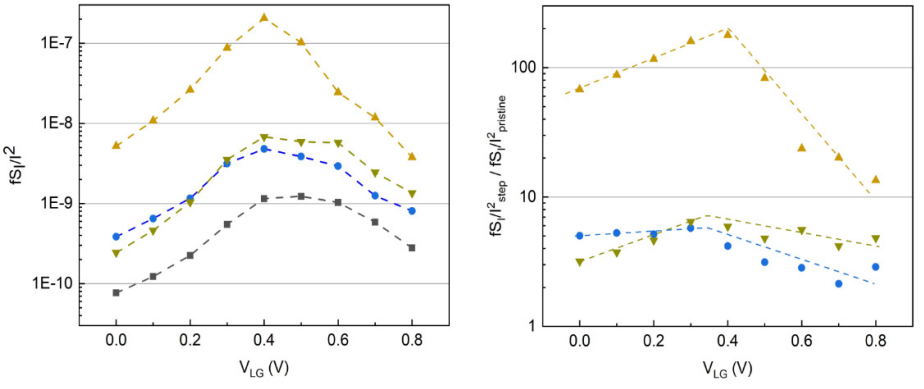

(a) (b)

Fig. 5. (a) Gate voltage dependence of the normalized noise power spectral density for each functionalization and immobilization step. (b) Relative change in noise amplitude normalized with respect to the gate-dependent noise of the pristine device. Key: black squares — pristine device (a); blue circles — after lipid monolayer formation; yellow upward triangles — after Ypt7 activation and attachment; green downward triangles — after HOPS complex immobilization (both (a) and (b)).

nanowire FET transducers showed similar effects of noise induced by analyte molecules present on the buffer side of the interface that were explained within the framework of the McWhorter model [17].

Therefore, we argue that the mechanism behind the changes in the noise spectra can be explained by changes in charge fluctuations upon functionalization, as discussed below.

The initial increase after the lipid monolayer formation can be attributed to charge fluctuations coupling to the transistor through the effective interface capacitance C_i [23].

The capacitance in liquid-gated GFETs typically consists of several components, including the electrical double-layer capacitance C_{EDL}, the quantum capacitance of graphene C_Q, and the air gap capacitance C_{airgap}, which are connected in series [1]. However, in the case of lipid-monolayer-functionalized GFETs, an additional capacitance component associated with the lipid layer C_{Lipids} must also be considered, leading to the modified interface capacitance equation:

$$\frac{1}{C_i} = \frac{1}{C_{\mathrm{EDL}}} + \frac{1}{C_Q} + \frac{1}{C_{\mathrm{airgap}}} + \frac{1}{C_{\mathrm{Lipids}}}. \tag{3}$$

Since C_{Lipids} dominates the total interface capacitance, it directly influences the input spectral power density, which can be expressed as $S_{\mathrm{input}} = (1/C_i)^2 S_q$, where S_q represents the power of random charge fluctuations caused by trap states at the graphene–lipid interface [23]. These trap states are considered to be the main contributors to the observed increase in fS_I/I^2.

While the exact origin of the transduction to the graphene channel remains unclear, we attribute the strong increase of $1/f$ noise to dynamic fluctuations of the Ypt7 protein, which might be inhibited after recruitment of the HOPS complex. These fluctuations may be caused by the *C*-terminal hypervariable domain (HVD) upstream of the prenylation motif of Ypt7. Importantly, the HVD is thought to be crucial for specific membrane targeting *in vivo* [24, 25].

Since the HVD is highly flexible, it is plausible that its dynamic motion near the membrane contributes to charge fluctuations and, consequently, the observed increase in $1/f$ noise.

On the other hand, the motion of the flexible HVD may cause fluctuations in the distance of the charged nucleotide binding pocket to the graphene channel. Previous studies showed that binding of the HOPS complex to Ypt7 induces an elongation of the HVD by approximately 0.7 nm [12]. The binding site of the HOPS complex in Ypt7 is thought to be near the nucleotide-binding pocket, in particular in close proximity to Switch I and Switch II. Therefore, the observed reduction in noise may result from either the stabilization of the HVD following elongation or from direct HOPS binding near the nucleotide pocket, suppressing previously observed charge fluctuation events. A combination of these factors may end Ypt7-induced noise, leading to the overall reduction in noise level. Further experimental validation is required to confirm this hypothesis and refine our understanding of the molecular dynamics governing membrane protein immobilization. Noise measurements on Ypt7 proteins with different lengths and flexibility of the HVD will be used to explore the molecular mechanism behind the charge fluctuations, while changing the anchoring of the Ypt7 within the lipid monolayer will allow for investigation of the transduction mechanism.

4. Conclusions

In this work, we successfully immobilized Ypt7 on GFETs functionalized with a lipid monolayer, which allowed us to explore the binding of the effector HOPS complex in a biological membrane environment. Interestingly, the *I*–*V* transfer characteristics and transconductance measurements showed no significant changes after HOPS immobilization. This limited response is likely due to the distant placement of HOPS from the graphene surface and, thus, depends on ionic conditions. Specifically, the Debye screening effect reduces the sensitivity of the device to electrostatic interactions at physiological ionic strengths. This finding suggests that tuning the ionic strength of the buffer could help improve signal detection in future experiments. However, changing the buffer concentration can severely affect the protein function.

On the other hand, noise spectroscopy revealed a much more pronounced and sensitive response to each functionalization step, such as lipid monolayer formation, protein immobilization, and protein–protein interaction. After forming the lipid monolayer, we observed an increase in noise, which we attribute to trap states forming at the graphene–lipid interface. Subsequent addition of Ypt7 leads to an

increase of $1/f$ noise by more than one order of magnitude, which is reduced to the previous level upon addition of the HOPS complex. The reduction in noise level is likely caused by the PPI between Ypt7 and the HOPS complex.

Our analysis points out two key regions of Ypt7 likely driving this effect: the nucleotide-binding pocket and the HVD. Both essential regions of the protein may be involved in random charge trapping and release events that contribute to the observed $1/f$ noise.

Altogether, our findings highlight the potential of combining lipid monolayer modification of GFETs with graphene-based noise spectroscopy as a highly sensitive approach for probing protein–membrane and PPI. Beyond basic research, this approach could be especially useful for studying molecular mechanisms of proteins that are associated with diseases related to membrane trafficking dysfunctions.

Acknowledgments

We acknowledge funding by the DFG in the framework of the RTG 2900 nanomaterials@biomembranes. CM, MF, and FS acknowledge DFG funding of instruments INST 190/189-1 and INST 190/190-1.

ORCID

M. Fomin https://orcid.org/0009-0003-4910-6367
F. Steinbach https://orcid.org/0009-0006-9958-7607
D. Pustovyi https://orcid.org/0000-0003-2838-6091
N. Füllbrunn https://orcid.org/0000-0003-1263-3166
C. You https://orcid.org/0000-0002-7839-6397
C. Ungermann https://orcid.org/0000-0003-4331-8695
S. Vitusevich https://orcid.org/0000-0003-3968-0149
M. Petrychuk https://orcid.org/0009-0009-2485-643X
C. Meyer https://orcid.org/0000-0003-0851-2767

References

[1] D. Kireev, M. Brambach, S. Seyock, V. Maybeck, W. Fu, B. Wolfrum and A. Offenhäusser, Graphene transistors for interfacing with cells: Towards a deeper understanding of liquid gating and sensitivity, *Sci. Rep.* **7** (2017) 6658, doi: 10.1038/s41598-017-06906-5.

[2] S. Szunerits, T. Rodrigues, R. Bagale, H. Happy, R. Boukherroub and W. Knoll, Graphene-based field-effect transistors for biosensing: Where is the field heading to?, *Anal. Bioanal. Chem.* **416** (2024) 2137–2150, doi: 10.1007/s00216-023-04760-1.

[3] M. Fomin, L. Jorde, F. Steinbach, C. You and C. Meyer, Liquid-gated graphene field-effect transistors for biosensing on lipid monolayers, *Phys. Status Solidi B* **260** (2023) 2300324, doi: 10.1002/pssb.202300324.

[4] L. Zuccaro, C. Tesauro, T. Kurkina, P. Fiorani, H. K. Yu, B. R. Knudsen, K. Kern, A. Desideri and K. Balasubramanian, Real-time label-free direct electronic monitoring of

topoisomerase enzyme binding kinetics on graphene, *ACS Nano* **9** (2015) 11166–11176, doi: 10.1021/acsnano.5b05709.

[5] Z. Wang, K. Yi, Q. Lin, L. Yang, X. Chen, H. Chen, Y. Liu and D. Wei, Free radical sensors based on inner-cutting graphene field-effect transistors, *Nat. Commun.* **10** (2019) 1544, doi: 10.1038/s41467-019-09573-4.

[6] R. Santos, O. Ursu, A. Gaulton, A. P. Bento, R. S. Donadi, C. G. Bologa, A. Karlsson, B. Al-Lazikani, A. Hersey, T. I. Oprea and J. P. Overington, A comprehensive map of molecular drug targets, *Nat. Rev. Drug Discov.* **16** (2017) 19–34, doi: 10.1038/nrd.2016.230.

[7] D. Nettels, N. Galvanetto, M. T. Ivanović, M. Nüesch, T. Yang and B. Schuler, Single-molecule FRET for probing nanoscale biomolecular dynamics, *Nat. Rev. Phys.* **6** (2024) 587–605, doi: 10.1038/s42254-024-00748-7.

[8] R. Qing, M. Xue, J. Zhao, L. Wu, A. Breitwieser, E. Smorodina, T. Schubert, G. Azzellino, D. Jin, J. Kong, T. Palacios, U. B. Sleytr and S. Zhang, Scalable biomimetic sensing system with membrane receptor dual-monolayer probe and graphene transistor arrays, *Sci. Adv.* **9** (2023) eadf1402, doi: 10.1126/sciadv.adf1402.

[9] O. Terral, G. Audic, A. Claudel, J. Magnat, A. Dupont, C. J. Moreau and C. Delacour, Graphene field-effect transistors for sensing ion-channel coupled receptors: Toward biohybrid nanoelectronics for chemical detection, *Adv. Electron. Mater.* **10** (2024) 2300872, doi: 10.1002/aelm.202300872.

[10] L. Jorde, Z. Li, A. Pöppelwerth, J. Piehler, C. You and C. Meyer, Biofunctionalization of carbon nanotubes for reversible site-specific protein immobilization, *J. Appl. Phys.* **129** (2021) 094302, doi: 10.1063/5.0035871.

[11] S. R. Tabaei, W. B. Ng, S.-J. Cho and N.-J. Cho, Controlling the formation of phospholipid monolayer, bilayer, and intact vesicle layer on graphene, *ACS Appl. Mater. Interfaces* **8** (2016) 11875–11880, doi: 10.1021/acsami.6b02837.

[12] N. Füllbrunn, Z. Li, L. Jorde, C. P. Richter, R. Kurre, L. Langemeyer, C. Yu, C. Meyer, J. Enderlein, C. Ungermann, J. Piehler and C. You, Nanoscopic anatomy of dynamic multi-protein complexes at membranes resolved by graphene-induced energy transfer, *eLife* **10** (2021) e62501, doi: 10.7554/eLife.62501.

[13] S. Kiontke, L. Langemeyer, A. Kuhlee, S. Schuback, S. Raunser, C. Ungermann and D. Kümmel, Architecture and mechanism of the late endosomal Rab7-like Ypt7 guanine nucleotide exchange factor complex Mon1–Ccz1, *Nat. Commun.* **8** (2017) 14034, doi: 10.1038/ncomms14034.

[14] A. S. Burguete, T. D. Fenn, A. T. Brunger and S. R. Pfeffer, Rab and Arl GTPase family members cooperate in the localization of the golgin GCC185, *Cell* **132** (2008) 286–298, doi: 10.1016/j.cell.2007.11.048.

[15] R. S. Goody, M. P. Müller and Y.-W. Wu, Mechanisms of action of Rab proteins, key regulators of intracellular vesicular transport, *Biol. Chem.* **398** (2017) 565–575, doi: 10.1515/hsz-2016-0274.

[16] M. J. Kirton and M. J. Uren, Noise in solid-state microstructures: A new perspective on individual defects, interface states and low-frequency $(1/f)$ noise, *Adv. Phys.* **38** (1989) 367–468, doi: 10.1080/00018738900101122.

[17] Y. Kutovyi, V. Piatnytsia, N. Boichuk, I. Zadorozhnyi, J. Li, M. Petrychuk and S. Vitusevich, Boosting the performance of liquid-gated nanotransistor biosensors using single-trap phenomena, *Adv. Electron. Mater.* **7** (2021) 2000858, doi: 10.1002/aelm.202000858.

[18] D. Shvarev, J. Schoppe, C. König, A. Perz, N. Füllbrunn, S. Kiontke, L. Langemeyer, D. Januliene, K. Schnelle, D. Kümmel, F. Fröhlich, A. Moeller and C. Ungermann, Structure of the HOPS tethering complex, a lysosomal membrane fusion machinery, *eLife* **11** (2022) e80901, doi: 10.7554/eLife.80901.

[19] M. Dankerl, M. V. Hauf, A. Lippert, L. H. Hess, S. Birner, I. D. Sharp, A. Mahmood, P. Mallet, J.-Y. Veuillen, M. Stutzmann and J. A. Garrido, Graphene solution-gated field-effect transistor array for sensing applications, *Adv. Funct. Mater.* **20** (2010) 3117–3124, doi: 10.1002/adfm.201000724.

[20] Y. Chen, Z. P. Michael, G. P. Kotchey, Y. Zhao and A. Star, Electronic detection of bacteria using holey reduced graphene oxide, *ACS Appl. Mater. Interfaces* **6** (2014) 3805–3810, doi: 10.1021/am500364f.

[21] N. Nekrasov, S. Jaric, D. Kireev, A. V. Emelianov, A. V. Orlov, I. Gadjanski, P. I. Nikitin, D. Akinwande and I. Bobrinetskiy, Real-time detection of ochratoxin A in wine through insight of aptamer conformation in conjunction with graphene field-effect transistor, *Biosens. Bioelectron.* **200** (2022) 113890, doi: 10.1016/j.bios.2021.113890.

[22] G. Palazzo, D. De Tullio, M. Magliulo, A. Mallardi, F. Intranuovo, M. Y. Mulla, P. Favia, I. Vikholm-Lundin and L. Torsi, Detection beyond Debye's length with an electrolyte-gated organic field-effect transistor, *Adv. Mater.* **27** (2015) 911–916, doi: 10.1002/adma.201403541.

[23] I. Heller, S. Chatoor, J. Männik, M. A. G. Zevenbergen, J. B. Oostinga, A. F. Morpurgo, C. Dekker and S. G. Lemay, Charge noise in graphene transistors, *Nano Lett.* **10** (2010) 1563–1567, doi: 10.1021/nl903665g.

[24] S. Pfeffer and D. Aivazian, Targeting Rab GTPases to distinct membrane compartments, *Nat. Rev. Mol. Cell Biol.* **5** (2004) 886–896, doi: 10.1038/nrm1500.

[25] P. Chavrier, J.-P. Gorvel, E. Stelzer, K. Simons, J. Gruenberg and M. Zerial, Hypervariable C-terminal domain of Rab proteins acts as a targeting signal, *Nature* **353** (1991) 769–772, doi: 10.1038/353769a0.